

Elastic constants and thermodynamics properties of pristine PEDOT revealed: A first-principles PBE/PBE PAW approach

R.O. Agbaoye¹, P.O. Adebambo², J.O. Akinlami¹, T.A. Afolabi³, S. Zh. Karazhanov⁴, D. Ceresoli^{5*} and G.A. Adebayo^{1*}

¹Department of Physics, Federal University of Agriculture, PMB 2240, Abeokuta, Nigeria

²Department of Physical and Computer Sciences, McPherson University, Abeokuta, Nigeria

³Department of Chemistry, Federal University of Agriculture, PMB 2240, Abeokuta, Nigeria

⁴Solar Energy Section, Institute for Energy, Norway

⁵CNR, Dipartimento di Chimica, Università degli studi di Milano via Golgi 19, 20133 Milano, Italy

ABSTRACT

In this work, we report for the first time, detailed calculations of elastic and thermodynamic properties of organic poly(3,4-ethylenedioxythiophene), PEDOT, in an undiluted state, using PBE and PBEsol-PAW pseudopotentials within the framework of Generalized Gradient Approximation Density Functional Theory. Contrary to Molecular Dynamic simulations, series of PBE and PBEsol-PAW calculations in the current work revealed the most stable state of monoclinic structured pristine PEDOT. We determined thirteen (13) independent elastic constants with elastic compliance which enables us to establish other elastic properties of pristine PEDOT; the Pugh's ratio and the Vicker's hardness calculations show small mismatches with PBE and PBEsol-PAW pseudopotentials. The Debye temperature T_D is predicted both in the PBE and PBEsol-PAW calculations while the specific heat capacity $C_v(T)$ follows the Dulong-Petit curve having no mismatch with Debye model at low temperature, with PBE predicting a higher Debye sound velocity than PBEsol-PAW. As accuracy tests only, we performed electronic structure calculations of PEDOT and compared with available data in the literature.

INTRODUCTION

Organic polymers, either in a pure or doped state are finding usefulness in solar cells and other modern day technologies due to their conductive and dispersive nature. In some, the optical transparency in the dispersion is very advantageous as these conductive organic polymers can serve as dichroic filters. Recent calculations by Wen Shi et al. provided electronic and thermoelectric properties of both pristine and doped PEDOT while Jun Liu et al. carried out experimental measurements of PEDOT-PSS (polystyrene sulfonate) mixture properties. Due to its flexible nature, thin film PEDOT-PSS is gaining broad applications in flexible electronic devices [1]. Since the first synthesis of PEDOT [2][3], several experimental studies and theoretical computations have been carried out on doped and pristine poly(3,4-ethylenedioxythiophene) either as thin-film or bulk material. These studies range from synthesis, doping, chemical preparation, thermoelectric properties to the electronic and optical structural determination. The conductivity, atmospheric stability, band gap, thermoelectric figure of merit among other properties of PEDOT have improved over time, but the elastic and thermodynamics properties have neither been studied nor reported until now.

As an organic semiconducting polymer, PEDOT is finding highly significant applications in modern day technology. It also serves as material to be doped with other polymers/materials to develop novel materials. These important attributes of PEDOT make it an important material to be studied both theoretically and experimentally. The semiconducting properties of PEDOT makes it a high efficient organic semiconductor. An important question therefore comes to mind as to whether there are other attributes of PEDOT that are responsible for its success as an organic semiconductor. To answer the question above, it is necessary to consider an alternative, but very important route to study the efficiency of PEDOT. Investigating the Elastic Constants, coupled with its Elastic compliance will shed more light on the reliability of PEDOT at various mechanical conditions.

As mentioned earlier, PEDOT is an optically active conductive conjugated polymer [4]. It exists as an organic semiconductor with a small direct band gap in the pure state; with exceptional environmental stability and electrical conductivity as well [5][6][7][8]. Synthesis in the pristine state via chemical polymerization results in blue-black colour with less transparency while it switches to almost transparent in the doped state [6][7]. The ability to change from benzoic shape to quinoid structure when doped with poly(styrene sulphurate) and also from aromatic like structure to quinoid like structure when doped with tosylate was reported by [9][10].

Organic pristine PEDOT semiconductor, when doped with a tosylate exhibits metallic tendency [10][11][12]. The gap between its highest occupied molecular orbital (HOMO) and its lowest unoccupied molecular orbitals (LUMO) is reported as 1.5eV, 1.6eV-1.7eV and 1.64eV [7][8][13] respectively. On the other hand, [10][11][12] reported gaps of 0.37eV with BLYP exchange-correlation functional, 0.45eV with PBE exchange-correlation functional, 0.16eV with PBE-D exchange-correlation functional and 0.53eV with HSE06 hybrid exchange-correlation functional. The discrepancy in the experimental and theoretical studies is due [7][8][13] to the fact that the studies are both on the thin film and bulk PEDOT.

It has been demonstrated that the band gap of bulk crystalline thin-film is less than that of nanocrystalline thin-film material [14]. In this regard, the band gap of a 2D system is less than that of a 1D system; this also explains the discrepancy in the band gap of the bulk and thin-film natural PEDOT material. Furthermore, the variation in the theoretical band gap is due to the different exchange-correlation term implemented in the various pseudopotentials from PBE, PBE-D, BLYP to HSE06 [10][11].

PEDOT possesses remarkable qualities with potential applications as an organic electronic component in the form of organic transistors, Organic Light Emitting Diodes (OLED), solid electrolytic capacitor, etc. [5][7][15]. It is also used in the production of Organic Optoelectronic and electro-optic conversion devices [5][7][8][11][15]. Recently, it has been used in biochemical response materials such as organic biosensors and chemical sensors [5][7][15]. It has also been used in nano-fibre electrode as well as textile fibres [5][7][9]. First-principles method enables to study the properties of materials to a high level of accuracy at specified temperature and pressure. Also, it is used to simulate non-existing materials with the aim of achieving optimised performance with less cost, little or no laboratory equipment and apparatus, in the comfort of one's computing device. The availability of high-performing clusters with hundreds of processors and high-level theoretical models for ions and electrons such as Density Functional Theory and Quasi-harmonic approximation amongst others has made it possible for calculating energy and forces of crystalline systems of tens or hundreds of atoms or molecules.

All of the above allow determination of many properties of a system which hitherto were hard to achieve. One of such is the elastic property with its 81 independent elastic constants and elastic compliances associated with a crystal. Using the approach employed by Newman, these are reduced to 21 for all crystal structure [16]; the symmetry operations of a monoclinic crystal contribute to reducing the 21 independent elastic constant and elastic compliances further to 13 which is sufficient to describe a monoclinic crystal structure, these elastic constants are:

$$C_{ij} = \begin{bmatrix} C_{11} & C_{12} & C_{13} & 0 & C_{15} & 0 \\ 0 & C_{22} & C_{23} & 0 & C_{25} & 0 \\ 0 & 0 & C_{33} & 0 & C_{35} & 0 \\ 0 & 0 & 0 & C_{44} & 0 & C_{46} \\ 0 & 0 & 0 & 0 & C_{55} & 0 \\ 0 & 0 & 0 & 0 & 0 & C_{66} \end{bmatrix}$$

1

Aside from the elastic constants, one can determine via first-principles method the Shear Modulus, Young modulus, Poisson Ratio, [16][17], bulk modulus [18]. The Poisson ratio shows the kind of bonding exhibit in a material and also determine its behaviour when a load is exerted on it [17]. A Poisson ratio near 0.33 characterised a material as having a strong metallic bond [18]. In fact, a Poisson ratio within the range 0.25-0.42 represents metals while in glasses, ceramics and semiconductors it tends to 0.25. Greaves and co-workers predicted a Poisson ratio approximately 0.33 in polymers [17].

Microscopically, the interaction of electrons and ions, as well as the extent of bonding between atoms are the cause of the behaviour of material to the external load. In PEDOT therefore, determination of the elastic properties is imperative in the production of bendable and flexible organic semiconductor materials.

COMPUTATIONAL DETAILS

Crystallographic information has described pristine PEDOT as having orthorhombic [11][12] as well as monoclinic crystal structures [10][11]. In the present work, we performed several optimised SCF calculations in Monoclinic phases of PEDOT. These calculations revealed the most stable phase of monoclinic pristine PEDOT. The monoclinic lattice parameters and atomic positions of the 52 atoms of pristine PEDOT were taken from the literature [10][11]. Pristine PEDOT has a space group P2/c [11] with space group number 13 having unique axis b [19]. We converted the obtained input cell dimensions into the unique monoclinic lattice parameters a, b and c, alpha, beta and gamma to define the initial monoclinic molecular crystal. We optimised the electronic cutoffwavefunction and charge density of the original configuration to 120Ry and 480Ry, 75Ry and 750Ry using Monkhorst pack kpoint grid 4*7*8 in PBE and PBEsol-PAW respectively. In determining the amount of kpoint required to determine the stable state of the molecular crystal, the Montkhorst pack kpoint grid was optimised by considering that size of the Brillouin zone in real space is an inverse of its size in reciprocal space. In monoclinic bravais lattice, the size of the Monkhorst Pack kpoint is non-uniform, since the size of its lattice parameters is not equal, this helped us determine the suitable number of kpoint within the available computation resources and not compromising accuracy.

As a result of huge computational cost, the atomic positions and lattice parameters a, b, and c we optimised using the BFGS quasi-newton algorithm with 2*4*4 Monkhorst pack kpoint grid. To reduce the force on the ions and to obtain the most stable state at minimum energy, the angle Beta between the lattice parameters a and b was optimised to achieve a global minimum state of the crystal using the 4*7*8 Monkhorst pack kpoint grid. We performed Self-Consistent Field Calculations with kpoint 6*10*11 and band structure calculations are carried out along the reciprocal coordinates of the high symmetry points Gamma-Y-Q-Z-Gamma-X. For the density of state, we performed Non-Self Consistent Field (NSCF) Calculations with a denser Monkhorst Pack kpoint grid of 7*11*12. We calculated the elastic constants of the molecular PEDOT by exerting strains that cause either longitudinal, transverse or both longitudinal and transverse distortion to the system, thereby calculating the stress that takes it back to its initial configuration, the strain and the obtained stress are then fitted to get the 13 independent elastic constants. To get more reliable results, we calculated the elastic constants within the 2*4*4, 3*5*5, 4*7*8, 5*8*9, 6*9*10 and 7,11,12 Monkhorst Park grid. In all, we sampled 18, 24, 72, 115 204, 258 kpoints and 20, 38, 114,

181, 332, 463 k-points for PBE and PBEsol-PAW respectively not minding the computational cost.

The elastic constants are calculated using the finite difference approach as implemented by Andrea Dal Corso [20]. According to him, for a small strain ϵ_j applied to perturb a crystal and the stress tensor σ_i that tends to return it to equilibrium, the little stress and the strain are related by:

$$\sigma_i = \sum_{j=1}^6 C_{ij} \epsilon_j \quad 2$$

this is analogous to Hooks law which describe the force required to extend or contract the size or shape of an elastic material, the crystal is perturbed by a set of 3*3 strain tensor which varies the length of lattice parameters, the size of the crystal along the yz, xz, xy planes, for a small applied strain of magnitude -0.0075, -0.0025, 0.0025 and 0.0075.

We perturbed the crystal by a set of 3*3 strain tensor which varies the length of lattice parameters, the size of the material along the yz, xz and xy planes (for a small applied) strain of magnitude -0.0075, -0.0025, 0.0025 and 0.0075 respectively. We performed this aspect of the calculations with the grimme-d2 semiempirical Van der Waal correction, norm-conserving Perdew-Burke-Enzenhoff and Ultrasoft Projected Augmented Wave pseudopotentials. We used a tolerance factor not more than 0.8meV/atom in the Monkhorst-Pack kpoint grid and the cutoff for wavefunction optimisations. Following the approach in literature [16][18][20], the elastic properties are calculated from Voigt-Heuss-Hill approximation.

The above approximation has proven to be a very useful method of determining the elastic properties of both organic and inorganic crystals [21] and is better than that employed by Guler [22]. We calculated the Bulk modulus, Young Modulus, Shear Modulus and the Poisson ratio of PEDOT using the approach described by [18][20][23]. Other calculated properties are the Pugh's Modulus ratio and Vicker's Hardness [1] [22][24][26].

We calculated the thermodynamic properties within the quasi-harmonic approximation as designed by Andrea Dal Corso. In the design, the internal energy and the Helmholtz free energy account for the optimised internal energy U_0 of the electron obtained from Density Functional Theory and its phonon contributions U_{ph} , F_{ph} ; therefore, Debye model was also instrumental in calculating the Debye temperature, average Debye speed of sound, Debye entropy, Debye vibrational free energy, Debye vibrational energy and Debye heat capacity.

$$U = U_0 + U_{ph} \quad 3$$

$$U_{ph} = \sum_{q,v} \frac{(\hbar\omega_{q,v})}{2} + \sum_{q,v} \frac{(\hbar\omega_{q,v} \beta \hbar\omega_{q,v})}{e} - 1 \quad 4$$

$$F = U_0 + F_{ph} \quad 5$$

$$F_{ph} = \sum_{q,v} \ln \left[2 \sinh \frac{(\beta \hbar\omega_{q,v})}{2} \right] \quad 6$$

Where \hbar , $\omega_{q,v}$ and β represent the Plank constant, Phonon frequency and Boltzmann constant respectively.

RESULT AND DISCUSSION

Table 1: The optimized lattice parameters of this study compared with other experimental and theoretical computation

Authors	Package	Exchange-correlation functional	a(\AA)	b(\AA)	c(\AA)	Beta (degree)
This work	Quantum Espresso	PBE (GGA)	10.773	7.878	7.445	123.0
This work	Quantum Espresso	PBESOL-PAW(GGA)	10.173	7.826	7.438	122.3
(Shi et al.,2015)	Vienna Ab initio Simulation Package	PBE-D (GGA)	12.0000	7.8200	7.0400	123.00
(Kim et al., 2008)	Car-Parrinello Molecular Dynamic	BLYP (GGA)	12.9780	7.9350	7.6000	125.85
(Tran-van et al., 2001)	Experimental	Spectroscopic and electrochemical study	10.5000	7.8700		

The optimised lattice parameters a and b using PBE exchange-correlation functional overestimate the experimental value while PBESol-PAW underestimates the experimental value. However, the lattice parameters a, b, c and beta computed with PBESol-PAW are less than that computed with PBE, but both are in agreement with other computational studies [26] on highly oriented pyrolytic graphite (HOPG) and diamond. In this study, the calculated structural optimisation maintained a decent accuracy of 2.6 percent error in lattice parameter a; 0.1 percent error in lattice parameter b with PBE exchange-correlation functional. On the other hand, a 3.1 percent error is recorded for lattice parameter a, 0.6 percent for lattice parameter b with PBESol-PAW exchange-correlation functional. Relatively, these errors are within acceptable limit compared to 14.3 percent with PBE-D exchange-correlation functional [10] and 23.6 percent using BLYP exchange-correlation functional [11]

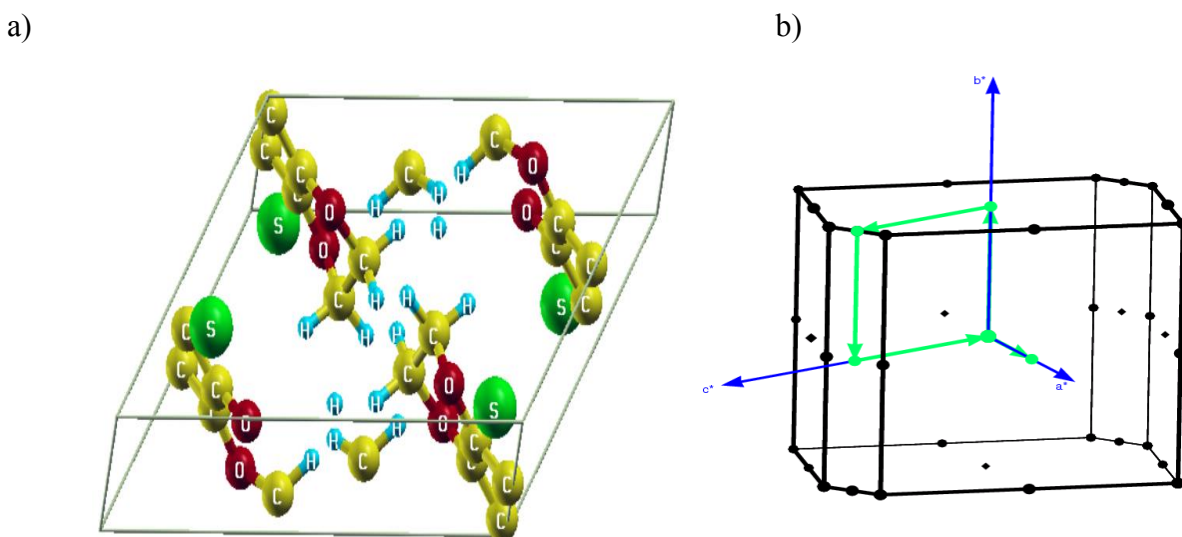


Figure 1: Crystal Structure and Brillion Zone of pristine pedot a) Crystal structure of pristine pedot,b) Brillion zone of pristine pedot showing the high symmetry points

The b unique monoclinic crystal structure of pristine PEDOT [10] consists of four molecules of ethylene dioxythiophene (EDOT) as illustrated in figure 1. The carbon, oxygen, sulphur and hydrogen atoms are shown with yellow, red, green and blue colours respectively. The individual EDOT molecules are seen clearly with its atoms bonding. Although a few atom is seen to have

fallen off the bond, this may be as a result of XCrySDen not capable of showing molecular crystal correctly or due to the slight change in atomic position as a consequence of the variable cell relaxation carried out to determine the minimum energy configuration of the molecular crystal. In figure 1b, the Brillouin zone along the high symmetry points from Gamma(0.0, 0.0, 0.0)-Y(0.0, 0.5, 0.0) – Q(0.0, 0.5, 0.5)- Z(0.0, 0.0, 0.5)-Gamma(0.0, 0.0, 0.0) – X(0.5 0.0 0.0) shows a segment of the Brillouin zone that represent all part of the Brillouin zone due to symmetry operations.

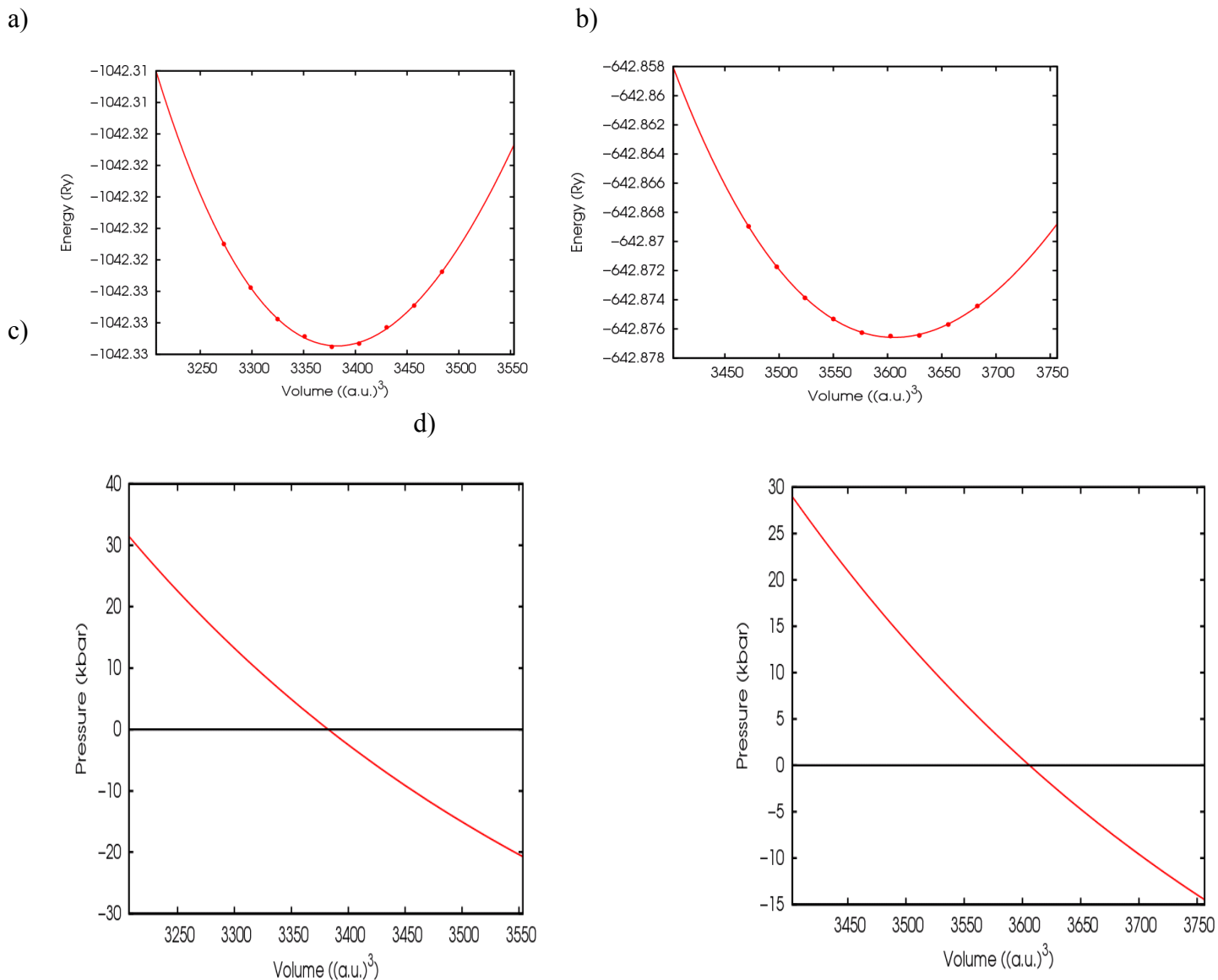


Figure 2: Volume optimization of pristine PEDOT: a) Energy- volume optimization using PBEsol-PAW b) Energy-Volume optimization using PBE c) Pressure -Volume optimization using PBEsol-PAW d) Pressure -Volume optimization using PBE

After obtaining the optimised lattice parameters a, b, c and beta, we determine the state at which pristine PEDOT is at its minimum energy configuration by determining its volume at the lowest energy of 3377.2 a.u and 3602.7 a.u. for PBEsol-PAW and PBE exchange-correlation functionals respectively. Furthermore, application of pressure on pristine PEDOT varies the Volume as shown in figure 2(c and d). At zero pressure, pristine PEDOT is in optimised or minimum energy state while applying positive pressure increases its Volume. Moreover, pressure application in the reverse direction makes it contract, hence the reduction in size as seen in figure 2(c and d; PBEsol-PAW and

PBE exchange-correlation functional respectively).

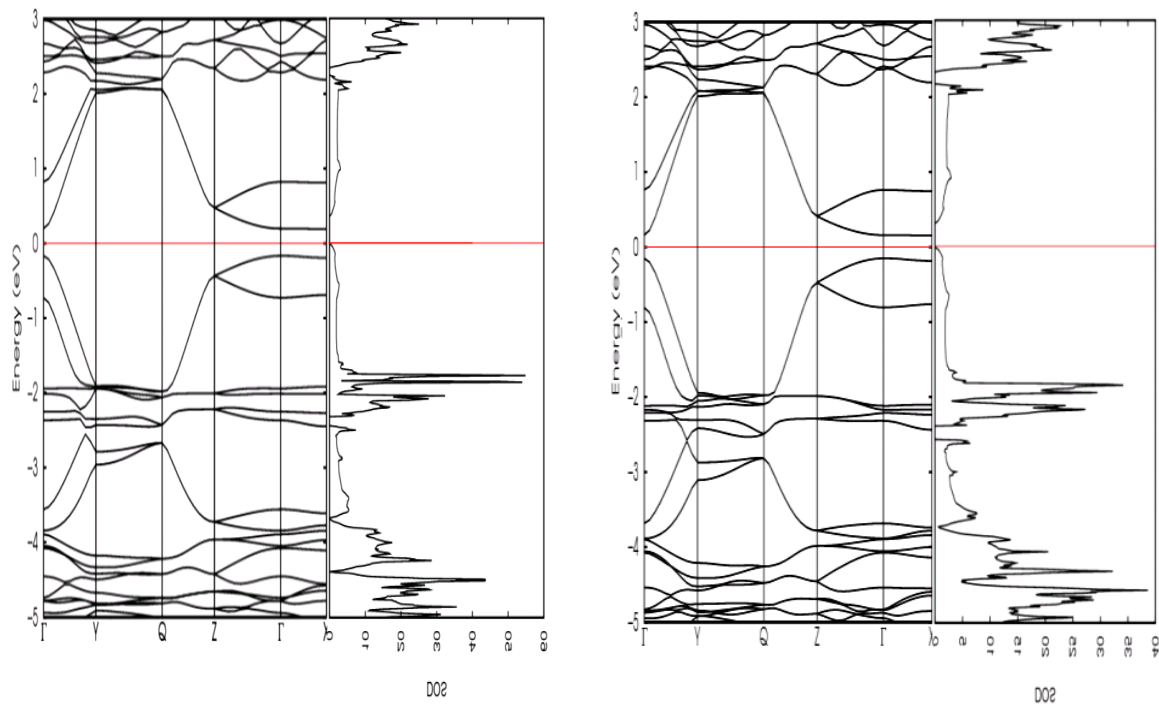


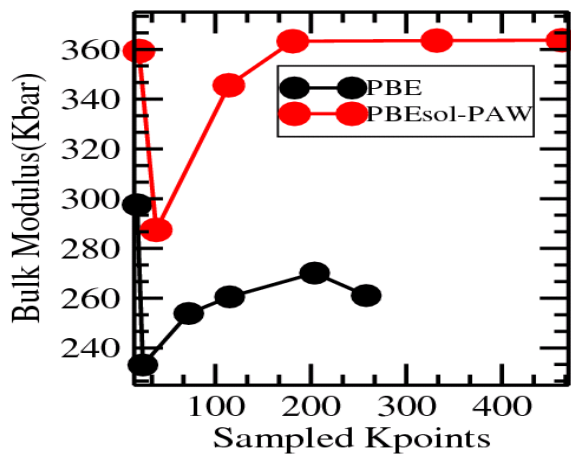
Figure 3: The Band structure and Density of state plot obtained using PBEsol-paw and PBE exchange-correlation functionals

We observed direct band gaps of 0.32eV and 0.42 respectively in Pbesol-PAW and PBE exchange-correlation functionals. In both functionals, flat-bands occur between 2 to 3eV and -4 to -5eV, which are due to the presence of dense electrons at those energy levels which manifest as sharp peaks in the density of state plot. The electrons are sparsely populated around the Fermi level causing the flat plot of the density of state and oval-shaped band from gamma to Z high symmetry point with significant gaps at Y and Q high symmetry points. Norm-Conserving Pseudopotentials produce a larger opening between split bands at Z-gamma-X around -2eV with less split opening recorded by the paw pseudopotential. These bands are similar to what was reported by [10][11][12]. In this work, PBE exchange-correlation functional produces a larger band gap. This variation in band gap is due to the difference in the exchange-correlation term supplied to the Kohn-Sham equation within DFT. Although there is no report on the experimental band gap of bulk pristine PEDOT, from the study of [27], PBEsol predicted a small band gap from DFT study of some oxyfluoride compounds. The calculated PBE and PBEsol-PAW band gaps in this work are in good agreements with 0.45eV reported by [12] and 0.37eV computed by [11]; although, far from 0.53eV and 0.16eV reported by [10].

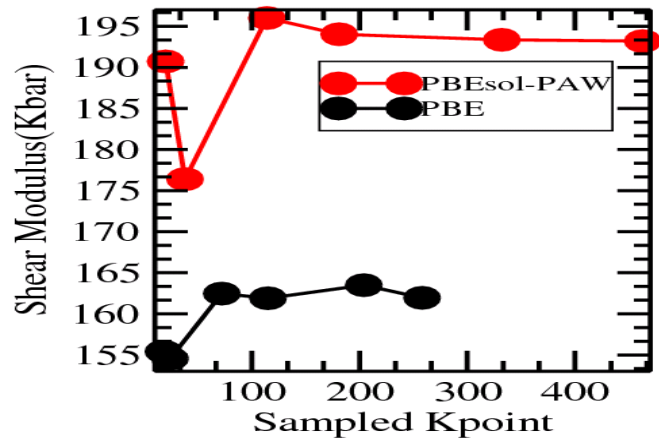
Table 2: Band gap comparison between this study and other experimental and theoretical computation for thin film and bulk PEDOT

Authors	package	Exchange-correlation functional	Type of Band PEDOT	Band gap(eV)	Type of Band Gap	Crystal structure
This work	Quantum Espresso	PBE (GGA)	Pristine PEDOT crystal	0.42	Direct band gap	Monoclinic
This work	Quantum Espresso	PBEsol-PAW(GGA)	Pristine PEDOT crystal	0.32	Direct band gap	Monoclinic
(Shi et al., 2015)	Vienna Ab initio Simulation Package	PBE-D (GGA)	Pristine PEDOT crystal	0.16	Direct band gap	Monoclinic
(Kim et al., 2008)	Car-Parrinello Molecular Dynamic	BLYP (GGA)	Pristine PEDOT crystal	0.37	Direct band gap	Orthorhombic
Zhang et al., 2015	CASTAP Molecular dynamic	PBE	Pristine PEDOT crystal	0.45	Direct band gap	Orthorhombic
Shi et al.,	Vienna Ab initio Simulation Package	HSE06	Pristine PEDOT crystal	0.5300		
(Tran-van et al., 2001) Shi et al., 2015	Experimental	Spectroscopic and electrochemical study	Thin film PEDOT	Approximately 1.7		
Havinga et al., 1996	Experimental	Vis-NIR Absorption spectra	PEDOT film	1.6400		
Pei et al (1994)	Experimental	Spectroscopy studies	Thin film PEDOT	1.5 and 1.6		

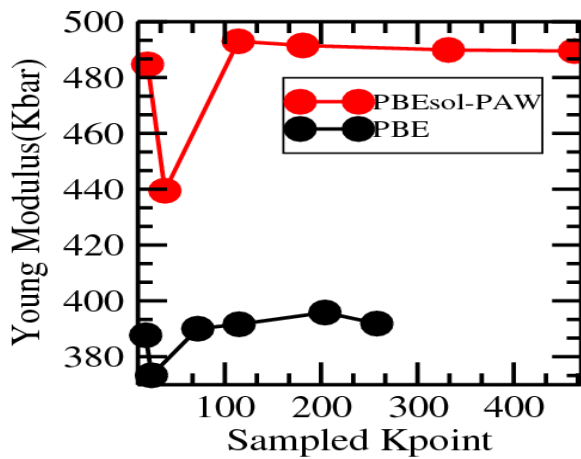
a)



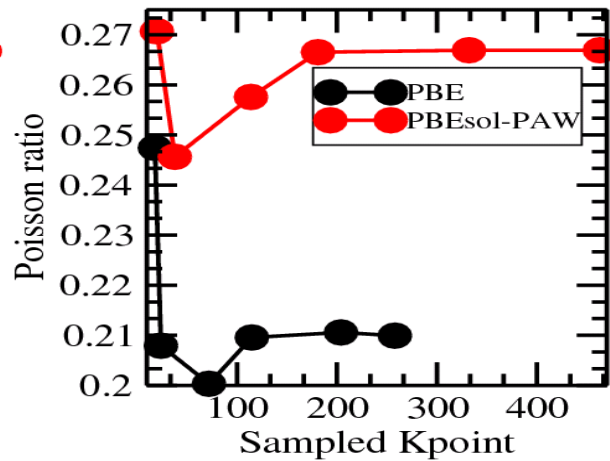
b)



c)

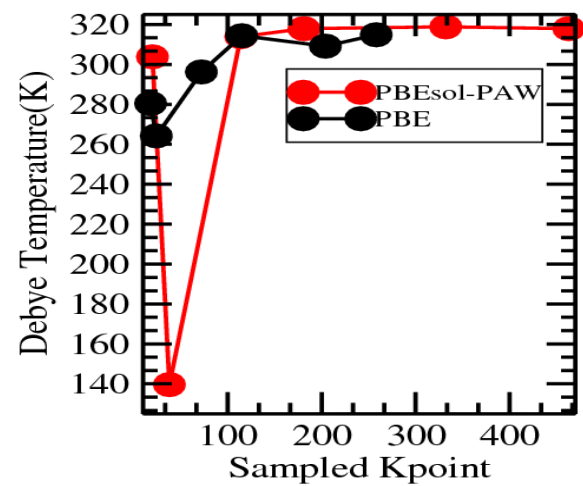
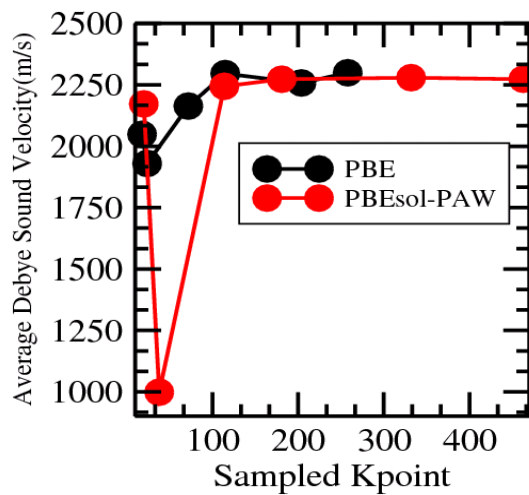


d)

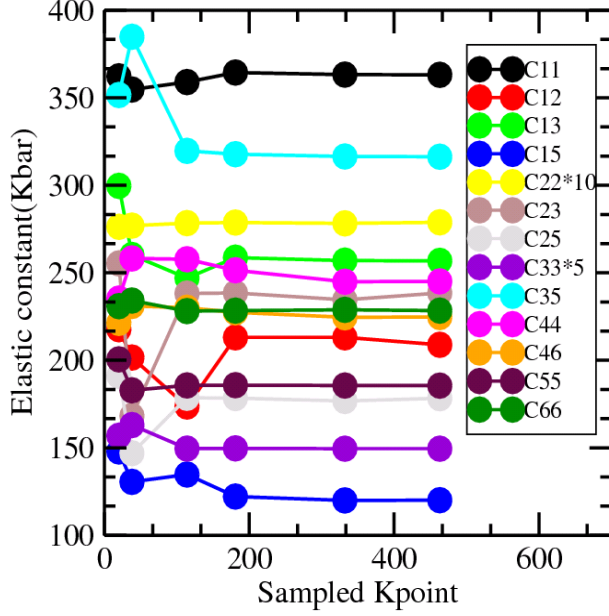


f)

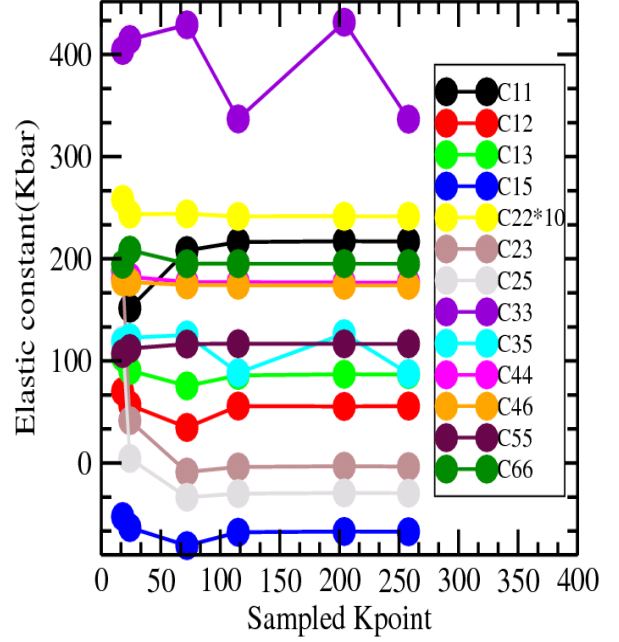
e)



g



h



The Figure 4: Elastic properties optimization with number of kpoints a) Bulk Modulus, b) Shear Modulus, c) Young Modulus and d) Poisson ratio e) Average debye sound velocity f) Debye temperature, colour red represent result from PBEsol-PAW while colour black shows result from PBE, g) represent the 13 independent elastic constant from PBEsol-PAW h) represent the 13 independent elastic constant from PBE.

Table 3: Bulk Modulus, Shear Modulus, Young Modulus, Poisson ratio Debye temperature and average Debye speed of sound for PBEsol-PAW and PBE exchange-correlation functional

	Bulk Modulus (Kbar)	Shear Modulus (Kbar)	Young Modulus (Kbar)	Poisson Ratio	Pugh Ratio	Vicker's Hardness (Kbar)	Debye Temperature (K)	Average debye speed of sound(m/s)
PBEsol-PAW	363.7	193.2	489.5	0.26690	0.5312	17.7	318	2272.469
PBE	261.0	161.9	391.9	0.20992	0.6203	19.4	315	2299.099

The Elastic constants, Bulk, Shear and Young Moduli, as well as the Poisson ratio, are calculated as described earlier; these carefully optimised results are with the size of the kpoint mesh within the Brillouin zone of the crystal. At an enormous computational cost, we realised that these results get exceptionally better with higher kpoint mesh. We, therefore, will like to stress further the importance of k-point sampling. Using an opinion from private communications, one can argue that for a given sampling, one requires a k-point mesh that depends effectively on the size of the reciprocal-space unit cell (i.e. Brillouin zone). A large real-space simulation cell will result in a small reciprocal-space cell, and consequently, one does not require a large k-point mesh [28].

According to Phillip, typically, in metallic systems and semiconductors/insulators k-point spacings range from $0.03 \times 2\pi/A$ (metallic) to $0.05 \times 2\pi/A$ (semiconducting/insulating systems) and will usually give an excellent quality sampling of the Brillouin zone. We found that for polymers such as PEDOT, the elastic constants and indeed, the elastic properties are hugely dependent on k-point sampling. Also, the contribution of information of a single k-point to the Brillouin zone as a whole can be described by the k-point weight, and we realised that calculations with N k-point would have all the k-points weighted by $1/N$ as well as the symmetries of PEDOT. Hence, our reasons to sample on $2*4*4$; $3*5*5$; $4*7*8$; $5*8*9$; $6*9*10$ and $7*11*12$.

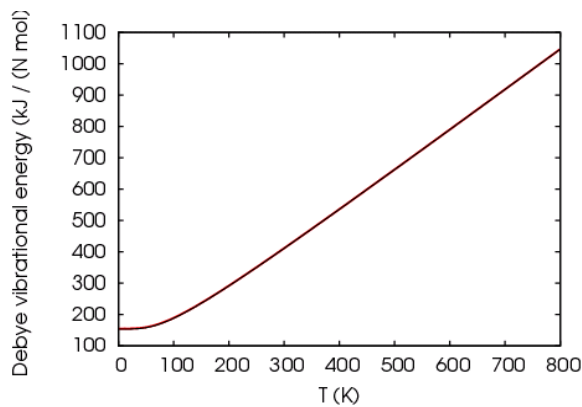
In PBEsol-PAW, optimised results occur with 463 sampled kpoints resulting in 0.08, 0, 0.03 and 0.08 percent difference in Shear Modulus, Poisson ratio, Bulk Modulus and Young Modulus respectively when compared with 332 kpoints, for the same Monkhorst Pack grid, Similarly, in PBE sampling at 258 sampled kpoints we have, 1, 0.3, 3.3 and 1 percent in Shear Modulus, Poisson ratio, Bulk Modulus and Young Modulus when compared with results from 204 kpoints. The Pugh ratio shows a disagreement on its brittleness as PBEsol-PAW categorise pristine PEDOT as ductile while PBE calculations predict a brittle material with a greater Vickers hardness. With a hardness of 1.77Kbar and 1.94Kbar, pristine PEDOT is far from that of diamond which is a super-hard material but has its hardness similar to that of ZnS with experimental Vicker's Hardness of 1.8Gpa [24][25]. Since the ratio of Bulk Modulus to Share Modulus is greater than unity, and the Poisson ratio tends weakly towards 0.5, we predict pristine PEDOT as mildly incompressible.

Table 4: The 13 independent elastic constants calculated using PBEsol-PAW and PBE exchange-correlation functionals

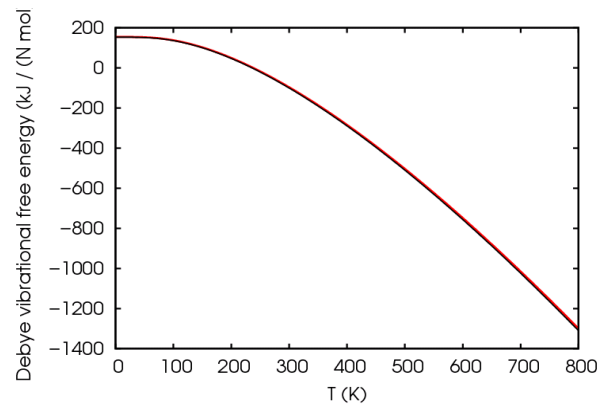
	C_{11}	C_{12}	C_{13}	C_{15}	C_{22}	C_{23}	C_{25}	C_{33}	C_{35}	C_{44}	C_{46}	C_{55}	C_{66}
PBEsol-PAW	363.1	208.9	256.9	120.1	2788.2	238.5	178.3	747.6	316.3	245.0	224.7	185.5	228.4
PBE	216.9	55.8	86.5	-67.3	2416.1	-3.4	-29.6	336.7	87.7	176.8	173.9	116.7	95.2

We optimised the 13 independent elastic constants with the number of kpoint. Although, we expect a slight difference in the elastic constants calculations both in PBEsol-PAW and PBE Pseudopotentials due to the differences in the size and volume of the crystal as reported in Table 1. We do not expect a large difference and negative elastic constants as seen in Table 4, The negative elastic constants can be interpreted as having the exerted stress compressing the crystal.

a)



b)



d)

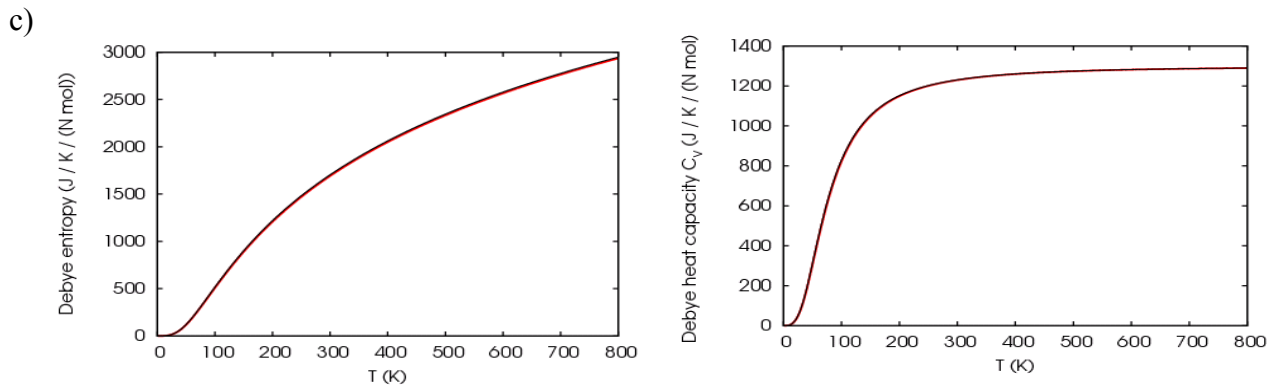


Figure 5: The Debye vibrational energy, Debye vibrational free energy, Debye entropy and Debye heat capacity obtained using PBEsol-PAW exchange-correlation functional
 The Debye vibrational energy, Debye vibrational free energy, Debye entropy and Debye heat capacity obtained using PBE exchange-correlation functional

The calculated Debye heat capacity at low temperatures $T \ll T_D$ accurately match [29] in both PBE and PBEsol-PAW calculation with Debye temperature T_D equals 315K and 318K. The Debye heat capacity tends towards the Dulong-petit model from 500K towards 800K where $T \gg T_D$; as expected the Debye entropy increases with temperature as the vibration of ions increases. There are no significant differences in the thermodynamic properties from PBE and PBEsol-PAW results because the exchange-correlation functional term of the Pseudopotential is only a factor in determining the electronic contribution as implemented in Density Functional Theory and not a factor in phonon contribution.

CONCLUSION

In the present study, we have carried out robust calculations to determine the optimised state, elastic properties as well as the thermodynamic properties of pristine PEDOT. Our results relatively compare well with available experimental data and better than other computational studies so far reported. For the sake of comparison, the band structure shape is similar to the ones reported by other computational studies, except for the different in band gap which is due to the different exchange-correlation functional used. Following the idea of Andrea Dal Corso, we realised that optimising the elastic constants and elastic properties improved our results drastically. The mismatch in the Pugh ratio that results in classifying pristine PEDOT as ductile and brittle with different Pseudopotentials is open to debate. We predicted pristine PEDOT is mildly incompressible and illustrated in the thermodynamic computations that increase in temperature causes steady increase in entropy, vibrational energy and heat capacity while the vibrational free energy reduces with temperature. The results of our calculations provide new physical insights to the mechanical properties of PEDOT via its elastic and thermodynamic properties and enable us to establish the elastic stability in pristine PEDOT. Other new insights include, the Pugh's ratio, Vicker's hardness, the Debye temperature, specific heat capacity.

ACKNOWLEDGEMENTS

The authors acknowledge the Abdus Salam International Centre for Theoretical Physics for computational access to its Clusters, ROA and GA are grateful to Ivan Giroto for assistance on resolving computational bugs.

*Author to whom all correspondences should be sent:

G.A. Adebayo* adebayo@physics.unaab.edu.ng

D. Ceresoli* davide.ceresoli@cnr.it

References

1. Zhou, J., Anjum D. H., Long C., Xuezhong X., Ventura I. A., Long J., Gilles L. The temperature-dependent microstructure of PEDOT/PSS films: insights from morphological, mechanical and electrical analyses. *J. Mater. Chem. C* 2014, 2 (46):9903.
2. Erez, D.I. Electrodepositing of PEDOT. Bachelor of Science Researchers thesis 2012
3. Cho, B.; Park, K.S.; Baek, J.; Oh, H.S.; Lee Y-E. K.; Sung, M. M. Single-Crystal Poly(3,4-ethylenedioxythiophene) Nanowires with Ultrahigh Conductivity *ASC/NanoLett* 2014 1-7
4. Cho W.; Wu J.; Shim B.S.; Kuan W.; Mastroianni S.E.; Young W.; Kuo C.; Epps T.H.; Martin D.C.; Synthesis and characterization of bicontinuous cubic Poly(3,4-ethylene dioxothiophene) gyroid (PEDOT GYR) gels, *Phys.Chem.Chem.Phys.*,2015, 17, 5115
5. Pyshkina O.; Kubarkov A.; Sergeev V., Poly(3,4-ethylenedioxythiophene):Synthesis and Properties. *Scientific Journal of Riga Technical University Material Science and Applied Chemistry*. 2010 21 51-54
6. Pei Q.; Zuccarello G.; Ahiskog M.; Inganas O. Electrochromic and highly stable Poly(3,4-ethylenedioxythiophene) switches between opaque blue-black and transparent sky blue. *Polymer* 1994 35:7 1347-1351
7. Tran-Van, F.; Garreau,S.; Louarn, G.; Froyer G. Chevrot, C. Fully undoped and soluble oligo(3,4-ethylenedioxythiophene)s: spectroscopic study and electrochemical characterization. *J. Mater. Chem.*, 2001, 11, 1378–1382
8. Aasmundtveit, K.E.; Samuelson, E.J.; Pettersson, L.A.A.; Inganas, O.; Johansson, T.; Feidenhans R. Structure of thin films of poly(3,4-ethylenedioxythiophene). *Synthetic Metals* 1999 101 561-564
9. Lenz, A.; Kariis, H.; Pohl, A.; Persson, P.; Ojamae L. The electronic structure and reflectivity of PEDOT: PSS from density functional theory. *Chemical Physics* 2011 384 44–51
10. Shi, W.; Zhao, T.; Xi, J.; Wang, D.; Shuai, Z. Unravelling doping effects on PEDOT at the molecular level: from geometry to thermoelectric transport properties. *J. AM. CHEM. SOC.* 2015 1-21
11. Kim, E.-G.; Bre´das J.-L. Electronic Evolution of Poly(3,4-ethylenedioxythiophene) (PEDOT): From the Isolated Chain to the Pristine and Heavily Doped Crystals. *J. AM. CHEM. SOC.* 2008, 130, 16880–16889
12. Zhang, B.; Wang, K.; Li, D.; Cui, X. Doping effects on the thermoelectric properties of the pristine Poly(3,4-ethylenedioxythiophene). www.rsc.org/advances 2015, 1-10
13. Havinga, E.E.; Mutsaers, C.M.J. Absorption Properties of Alkoxy-Substituted Thiophene-Vinylene Oligomers as a Function of the Doping Level. *Chem. Mater.* 1996, 8, 769-776
14. Das, R.; Pandey, S. Comparison of Optical Properties of Bulk and Nano Crystalline Thin Films of CdS Using Different Precursors. *IJMS* 2011 1,1 35-40
15. Cho W.; Wu J.; Shim B.S.; Kuan W.; Mastroianni S.E.; Young W.; Kuo C.; Epps T.H.; Martin D.C.; Synthesis and characterization of bicontinuous cubic poly(3,4-ethylene dioxothiophene) gyroid (PEDOT GYR) gels, *Phys.Chem.Chem.Phys.*,2015, 17, 5115
16. Newman E. R. *Properties of Materials Anisotropy, Symmetry, Structure*, (Oxford University Press New York 2005)
17. Greaves, N G.; Greer, A. L.; Lakes, R.S.; Rouxel, T. Poisson's ratio and modern materials *Nature Materials* VOL 10 2011 823-837 Comparison of Optical Properties of Bulk and Nano

Crystalline Thin Films of CdS Using Different Precursors

18. Li, Y.; Gao, Y.; Xiao, B.; Min, T.; Yang, Y.; Ma, S.; Yi, D.; The electronic, mechanical properties and theoretical hardness of chromium carbides by first-principles calculations *Journal of Alloys and Compounds* 509 2011 5242–5249
19. M. I. Aroyo, A. Kirov, C. Capillas, J. M. Perez-Mato & H. Wondratschek Bilbao Crystallographic Server II: Representations of crystallographic point groups and space groups" *Acta Cryst. A* 62, 2006 115-128. doi:10.1107/S0108767305040286
20. Dal Corso, A. 2016. Elastic constants of beryllium: a first-principles investigation. *Journal of Physics: Condensed Matter*. *J.Phys.:Condens.Matter* 28 2016 075401
21. Yao, H.; Ouyang, L. Ching, W.-Y. Ab Initio Calculation of Elastic Constants of Ceramic Crystals. *Am. Ceram. Soc.*, (2007) 90 [10] 3194–3204
22. Guler, E.; Guler, M. Elastic and Mechanical Properties of Cubic Diamond under Pressure *CHINESE JOURNAL OF PHYSICS* 2015 53: 2 040807-1 - 040807-11
23. Shahsavari, R.; Buehler, M.J.; Pellenq, R.J.-M.; Ulm, F.-J. First-Principles Study of Elastic Constants and Interlayer Interactions of Complex Hydrated Oxides: Case Study of Tobermorite and Jennite. *J. Am. Ceram. Soc.*, 92 [10] 2323–2330.
24. Tian, Y.; Xu, B.; Zhao, Z. Microscopic theory of hardness and design of novel superhard crystals. *Int. Journal of Refractory Metals and Hard Materials* 2012 33 93–106
25. Chen, X.-Q.; Niu, H.; Li, D.; Li, Y. Modeling hardness of polycrystalline materials and bulk metallic glasses. *Intermetallics* 2011 19 1275-1281
26. Lechner C.; Pannier, B; Baranek, P; Forero-Martinez, N.C.; Vach H. First-Principles Study of the Structural, Electronic, Dynamic, and Mechanical Properties of HOPG and Diamond: Influence of Exchange–Correlation Functionals and Dispersion Interactions. *J. Phys. Chem* 2016 A-R
27. Charles, N.; and Rondinelli, J. M. Assessing exchange-correlation functional performance for structure and property predictions of oxyfluoride compounds from first principles. arXiv:1608.04450v1 [cond-mat.mtrl-sci] 16 Aug 2016
28. Phillip J. Hasnip, in private communications and in ResearchGate, October 2016.
29. Wallace D.C. *Thermodynamics of crystal*. John Willey and Sons Inc. 1972.